DISCRETE AND CONTINUOUS
DYNAMICAL SYSTEMS SERIES B
Volume **11**, Number **2**, March **2009**

doi:10.3934/dcdsb.2009.11.497

pp. **497–517**

SHEARED NEMATIC LIQUID CRYSTAL POLYMER MONOLAYERS

Hongyun Wang

Department of Applied Mathematics and Statistics
University of California, Santa Cruz, CA 95064, USA

Hong Zhou

Department of Applied Mathematics
Naval Postgraduate School, Monterey, CA 93943, USA

M. Gregory Forest

Department of Mathematics & Institute for Advanced Materials
University of North Carolina, Chapel Hill, NC 27599-3250, USA

(Communicated by Qi Wang)

Abstract. We provide a comprehensive study on the planar (2D) orientational distributions of nematic polymers under an imposed shear flow of arbitrary strength. We extend previous analysis for persistence of equilibria in steady shear and for transitions to unsteady limit cycles, from closure models [21] to the Doi-Hess 2D kinetic equation. A variation on the Boltzmann distribution analysis of Constantin *et al.* [3, 4, 5] and others [8, 22, 23] for potential flow is developed to solve for all persistent steady equilibria, and characterize parameter boundaries where steady states cease to exist, which predicts the transition to tumbling limit cycles.

1. **Introduction.** Macromolecular materials (for example, nematic liquid crystal polymers (LCP)) exhibit large flexibility and can be easily processed into fibers with high strength, or thin films [1, 6, 26]. The bulk properties of these materials are closely related to the processing flows. So it is very important to understand the dynamic behavior of the materials in the presence of flows.

The kinetic Doi-Hess theory [7, 17] has been a popular model for nematic LCPs. In kinetic theory each nematogenic molecule is coarse grained as a rigid rod and the ensemble is described by an orientational probability density function (pdf) which evolves according to the Smoluchowski (or Fokker-Planck) equation. Theoretical investigations have been carried out for pure nematic equilibria [3, 4, 5, 8, 22, 23, 29], extensional flow-induced equilibria [27], stable equilibria of dipolar ensembles [19, 30], effect of high [24, 25, 28] and weak shear [31], and effect of coplanar magnetic field [16]. Numerical simulations of the Smoluchowski equations can be found in [2, 9, 10, 11, 12, 13, 14, 15, 18, 20]. The first 3-D simulations carried out by Larson [20] showed shear-induced transitions and confirmed Marrucci and Maffettone's 2-D calculations [24, 25].

2000 *Mathematics Subject Classification.* Primary: 82D60, 76A15; Secondary: 65Z05, 35Q99.
Key words and phrases. Shear flow, nematic liquid crystal polymers, phase diagram.

In the 2-D case, it is well-known that in the absence of flow the isotropic-nematic phase transition occurs at $U = 2$, where U is the normalized polymer concentration. In the presence of an imposed weak shear there is a threshold ($U_0 \approx 2.41144646$) for U: When $U < U_0$, steady state solution exists; otherwise there is no steady state and the orientational pdf is temporally periodic ("tumbling") and can never reach a steady state.

The goal of this work is to conduct a comprehensive study of the 2-D nematic liquid crystal polymers under an arbitrary shear. In [21] monolayer films of liquid crystal polymers have been modeled with a mesoscopic two-dimensional (2D) analogue of the Doi-Hess kinetic model. The weak-shear steady and unsteady selection criteria for 2D nematic polymers using various second-moment closures was derived. A simple proof was given based on the Poincare-Bendixon Theorem to show that limit cycles ("tumbling orbits") exist beyond the parameter boundary for the steady-unsteady transition. Finally, it was revealed that the shear-perturbed 2D phase diagram is significantly robust to closure approximations than the 3D system. Our approach here differs from [21] in that we use the kinetic Smoluchowski equation instead of the Doi tensor model. There are two minor differences between our work and [21]. 1) In [21], a bistable region (where there are two stable solutions) was observed for the Doi closure tensor model. In our study using the full Smoluchowski equation there is no bistable region. Note that the bistable region in [21] is extremely small and it is difficult to pinpoint what small differences between the full Smoluchowski model and closure-based tensor models might cause this small bistable region. 2) In [21], Bogdanov-Takens bifurcation was observed whereas there is no Bogdanov-Takens bifurcation in our study. Again note that in [21] the Bogdanov-Takens bifurcation occurs in a very narrow region in the phase diagram. Our results are in general consistent with those in [21] in several aspects: 1) Both models identify critical values of polymer concentration, beyond which there is no steady state; 2) Both models yield the fold structure in the phase diagram. However, a detailed fold structure is resolved in this work. Specifically, the fold is not a kink, rather it is a smooth turn with large curvature. Furthermore, we find that fold structure in the phase diagram (the plot of order parameter versus U) exits for $Pe < 0.746$. For $Pe > 0.746$, the fold structure disappears. At the critical value of $Pe \approx 0.746$, the boundary separating the steady state region and the tumbing region in the $Pe - U$ plane appears to have a singularity. In [21] it was mentioned that unstable state can be further classified as tumbling or wagging. Tensor models were originally motivated by the fact that in the Doi-Hess kinetic model with the Maier-Saupe potential, an equilibrium state is completely specified by the orientation tensor. As a result, tensor models can provide good approximations at equilibrium or near equilibrium. In 2-D tensor models the system state is represented by the orientation direction and the order parameter. Thus, it is natural to try to classify time-periodic unsteady state as tumbling or wagging. If the director rotates continuously in one direction, we may say it is tumbling; if the director moves back and forth in a certain range, we may say it is wagging. Even in the tensor models, such a classification may be problematic since the director angle is undefined at the isotropic state. If the time-periodic evolution ever goes through the isotropic state, such a classification may be vague. It is worthwhile to note that "tumbling" refers to the tumbling of the orientation probability density. As for individual polymer rods, under a shear they are always tumbling in the direction of shear even if the orientation pdf is in a steady state. With a full Smoluchowski

equation (i.e. the Doi-Hess model),we find that under a weak shear the orientation probability density function (pdf) is a traveling wave with the location-dependent velocity, that is, the shape of the orientation pdf is maintained while the whole function may shift in the orientation dimension. So in the case of weak shear, the classification of tumbling and wagging makes perfect sense. But in the case of weak shear, it was found that there is only tumbling and there is no wagging [31]. As Pe gets larger (i.e. the shear getting stronger), the unsteady evolution of the orientation pdf becomes more complicated. As the peak of the pdf moves, the shape of the pdf changes dramatically for large Pe. We feel that the classification of tumbling and wagging is no longer adequate for providing a good picture of the time-evolution of the orientation pdf. We will pursue a comprehensive classification of the pdf in the future work. Here we shall refer the time-periodic unsteady state simply as tumbling.

In this paper we present and discuss phase diagrams for a very wide range of the Peclet number. For small Peclet number, the result of the current analytical/numerical study confirms the conclusions of the previous asymptotic study [31]: When the concentration parameter U is greater than a critical value U_0 (≈ 2.41144646), there is no stable steady state; when U is smaller than U_0, there is one stable branch of steady state; the stable branch and an unstable branch form a fold and are connected at U_0. The current study resolves the details of the transition from stability to instability along the phase diagram: the transition occurs around the folding point of the phase curve. As the Peclet number increases, the stable branch and the unstable branch of the fold are peeled off from each other and are separated. For $Pe > 0.746$, the fold disappears completely, that is, the phase curve no longer has a folding point. Furthermore, for $Pe > 0.746$, there is only one steady state (stable or unstable) for each value of U, and the transition from stability to instability occurs at a Hopf bifurcation point.

2. **Two-Dimensional formulation.**

We start with reviewing the mathematical formulation of the Doi-Hess kinetic theory for two-dimensional homogeneous flows of rigid rodlike molecules immersed in a viscous solvent subject to an imposed flow field [7, 17]. The orientation of a polymer rod is described by an angle θ and the orientational direction of each polymer rod is denoted by $\mathbf{u} = (\cos\theta, \sin\theta)$.

We consider the steady state solution of the Smoluchowski equation in the form [7]

$$\frac{\partial \rho}{\partial t} = \frac{\partial}{\partial \theta}\left[(-f + \psi^{'}(\theta))\rho + \frac{\partial}{\partial \theta}\rho\right], \tag{1}$$

where $\rho(\theta, t)$ is the orientational probability density function of the ensemble, $\psi(\theta)$ is a periodic function with period π, and f is a constant torque. In the case of nematic polymers under shear, $\psi(\theta)$ contains both the Maier-Saupe interaction and the effect of the elongational component of the shear whereas f is caused by the rotational component of the shear. The steady state solution satisfies

$$(-f + \psi^{'}(\theta))\rho + \frac{\partial}{\partial \theta}\rho = -J, \tag{2}$$

where J is the steady state probability flux. Multiplying (2) by the integrating factor $\exp[-f\theta + \psi(\theta)]$, we have

$$\frac{\partial}{\partial \theta}\left[\exp(-f\theta + \psi(\theta))\rho\right] = -J\exp\left[-f\,\theta + \psi(\theta)\right]. \tag{3}$$

Integrating from θ to $\theta+\pi$ yields

$$[\exp(-f\pi)-1]\exp[-f\theta+\psi(\theta)]\rho(\theta) = -J\int_{\theta}^{\theta+\pi}\exp[-f\bar{\theta}+\psi(\bar{\theta})]d\bar{\theta}. \tag{4}$$

Solving for $\rho(\theta)$ gives

$$\rho(\theta) = \frac{J}{1-\exp(-f\pi)}\exp[-\psi(\theta)]\int_{0}^{\pi}\exp[-f\bar{\theta}+\psi(\theta+\bar{\theta})]d\bar{\theta}. \tag{5}$$

The value of the probability flux J is determined from the condition

$$\int_{0}^{\pi}\rho(\theta)d\theta = 1. \tag{6}$$

Note that once we know f and $\psi(\theta)$, the probability density $\rho(\theta)$ is conveniently determined from (5). An efficient method of implementing (5) based on the Fast Fourier Transform (FFT) is discussed in Appendix A.

When an external shear flow with arbitrary strength is imposed, the Smoluchowski equation (1) can be written as

$$\frac{\partial\rho}{\partial t} = \frac{\partial}{\partial\theta}\left[(-\frac{Pe}{2}+V_{SH}^{'}(\theta)+V_{MS}^{'}(\theta))\rho+\frac{\partial}{\partial\theta}\rho\right], \tag{7}$$

where $Pe=\gamma/Dr$ is the Peclet number, a nondimensional parameter measuring the relative strength of viscosity (γ) and rotational diffusivity (Dr). In equation (7), $V_{SH}(\theta)$ is the periodic part of the potential induced by the imposed shear,

$$V_{SH}(\theta) = \frac{Pe}{4}\sin 2\theta, \tag{8}$$

and $V_{MS}(\theta)$ is the Maier-Saupe short-range interaction potential,

$$V_{MS}(\theta) = -U\langle\cos 2(\theta-\alpha)\rangle\cos 2(\theta-\alpha), \tag{9}$$

where the brackets $\langle\cdot\rangle$ denote the ensemble average with respect to the probability density function $\rho(\theta)$ and the angle α is selected such that

$$\langle\sin 2(\theta-\alpha)\rangle = 0. \tag{10}$$

Let $r\equiv U\langle\cos 2(\theta-\alpha)\rangle$. With the introduction of r, the Maier-Saupe potential can be expressed as

$$V_{MS}(\theta) = -r\cos 2(\theta-\alpha) \tag{11}$$

and the order parameter can be written as

$$\langle\cos 2(\theta-\alpha)\rangle = \frac{r}{U}. \tag{12}$$

Note that equation (1) reduces to (7) if we use the substitutions $f=\frac{Pe}{2}$ and

$$\begin{aligned}\psi(\theta) &= \frac{Pe}{4}\sin 2\theta - r\cos 2(\theta-\alpha)\\ &= \frac{Pe}{4}\cos 2\alpha\sin 2(\theta-\alpha) - (r-\frac{Pe}{4}\sin 2\alpha)\cos 2(\theta-\alpha)\\ &= \frac{Pe}{4}\cos 2\alpha\sin 2(\theta-\alpha) - q\cos 2(\theta-\alpha)\end{aligned} \tag{13}$$

where

$$q = r-\frac{Pe}{4}\sin 2\alpha. \tag{14}$$

It is clear that once the values of Pe, r and α are given, the total potential is completely specified and the steady state probability density (if a steady state exists)

is given by (5). The existence of steady state solution of the Smoluchowski equation (7) depends on the existence of solution of the following nonlinear system:

$$\begin{aligned} F_1(\alpha, q, Pe) &\equiv \langle \sin 2(\theta - \alpha)\rangle = 0, \\ F_2(\alpha, q, Pe) &\equiv \langle \cos 2(\theta - \alpha)\rangle = \frac{r}{U}, \end{aligned} \tag{15}$$

where the pdf used in averaging is the one given in (5). In the nonlinear system (15), Pe and U are parameters whereas r and α are unknowns. Alternatively, q and α can be used as unknowns where q and r are related by (14).

The goal of this paper is to study the existence and stability of steady solutions of the nonlinear system (15) for $Pe > 0$ and $U > 0$. It is worth noticing that with the introduction of r, the pdf given in (5) is independent of U. So we can avoid the parameter U in our analysis until the very end. These are the big advantage and mathematical convenience of dealing with r instead of U.

3. **Existence of steady state solutions.** In this section we will study (both analytically and numerically) the existence of solutions of the nonlinear system (15) with $0 < U < \infty$ for a given value of Pe. It is important to keep in mind that the pdf in (5) is independent of U with the use of r.

Since $\sin 2\theta$ is a periodic function with period π, we can restrict the range of α to $[-\frac{\pi}{4}, \frac{3\pi}{4}]$. Also note that $\sin 2\theta$ satisfies

$$\begin{aligned} \sin 2\left[\theta - (\alpha + \frac{\pi}{2})\right] &= \sin\left[2(\theta - \alpha) + \pi\right] \\ &= -\sin 2(\theta - \alpha), \\ \cos 2\left[\theta - (\alpha + \frac{\pi}{2})\right] &= \cos\left[2(\theta - \alpha) + \pi\right] \\ &= -\cos 2(\theta - \alpha). \end{aligned}$$

That is, the polymer orientation distribution with order parameter $\langle \cos 2(\theta - \alpha)\rangle$ and phase angle α is identical to the polymer orientation distribution with order parameter $-\langle \cos 2(\theta - \alpha)\rangle$ and phase angle $\alpha + \pi/2$. So by allowing $r \equiv U\langle \cos 2(\theta - \alpha)\rangle$ to be both positive and negative, we can further restrict the range of α to $[-\frac{\pi}{4}, \frac{\pi}{4}]$.

We first make a change of variable $\theta_{new} = \theta - \alpha$. For simplicity, we still denote the new variable θ_{new} by θ and the corresponding pdf and potential for the new variable θ_{new} by $\rho(\theta)$ and $\psi(\theta)$, respectively. In our notation, (15) becomes

$$F_1(\alpha, q, Pe) \equiv \langle \sin 2\theta\rangle = 0, \tag{16}$$

$$F_2(\alpha, q, Pe) \equiv \langle \cos 2\theta\rangle = \frac{r}{U}, \tag{17}$$

where the new pdf $\rho(\theta)$ and the new potential $\psi(\theta)$ are

$$\rho(\theta) \propto \exp[-\psi(\theta)] \int_0^{\pi} \exp[-\frac{Pe}{4}\bar{\theta} + \psi(\theta + \bar{\theta})]d\bar{\theta}, \tag{18}$$

$$\psi(\theta) = \frac{Pe}{4}\cos 2\alpha \sin 2\theta - q\cos 2\theta. \tag{19}$$

For a given value of Pe, the function $F_1(\alpha, q, Pe)$ depends on only q and α. Our extensive numerical calculations suggest that for any value of $Pe > 0$ and any value of $\alpha \in [-\frac{\pi}{4}, \frac{\pi}{4}]$, there exists one and only one value of q such that $F_1(\alpha, q, Pe) = 0$.

A rigorous mathematical proof of the uniqueness is still open. In Appendix B, we prove the existence by showing the asymptotic behaviors of $F_1(\alpha, q, Pe)$:

$$F_1(\alpha, q, Pe) = \begin{cases} Pe(1-\cos 2\alpha)\dfrac{1}{4q} + \cdots > 0, & \text{if } \cos 2\alpha < 1, \\ \dfrac{Pe}{8q^2} + \cdots > 0, & \text{if } \cos 2\alpha = 1, \end{cases} \quad \text{as } q \to +\infty,$$

$$F_1(\alpha, q, Pe) = Pe(1+\cos 2\alpha)\frac{1}{4q} + \cdots < 0, \quad \text{as } q \to -\infty.$$

Since $F_1(\alpha, q, Pe)$ is continuous and it has opposite sign at positive and negative infinity, there exists a point such that it is zero. In other words, equation (16) can always be satisfied and for a fixed value of Pe it defines uniquely a function $q(\alpha)$ such that $F_1(\alpha, q(\alpha), Pe) = 0$. Notice that in (16)–(19), α appears only in the potential $\psi(\theta)$ in the form of $\cos 2\alpha$. Since $\cos 2\alpha$ is an even function with respect to α, the whole problem (16)-(19) is even with respect to α. Consequently, $q(\alpha)$ is an even function of α.

Now, in potential $\psi(\theta)$ given in (19), we replace q by function $q(\alpha)$. It follows that for a fixed value of Pe, the pdf $\rho(\theta)$ given in (18) is now a function of α only for $\alpha \in [-\frac{\pi}{4}, \frac{\pi}{4}]$.

For mathematical convenience, let us introduce several functions as follows:

$$\begin{aligned} r(\alpha) &\equiv q(\alpha) + \frac{Pe}{4}\sin 2\alpha, \\ s(\alpha) &\equiv F_2(\alpha, q(\alpha), Pe), \\ w_0(\alpha) &\equiv \frac{q(\alpha)}{s(\alpha)}, \\ w(\alpha) &\equiv \frac{r(\alpha)}{s(\alpha)} = w_0(\alpha) + \frac{Pe}{4}\cdot\frac{\sin 2\alpha}{s(\alpha)}. \end{aligned}$$

As we discussed earlier, the function $s(\alpha)$ is also an even function of α. As we will see later, the nonlinear system (16) and (17) governing the steady state solutions can be conveniently described by these introduced functions. Furthermore, the nonlinear system (16) and (17) in terms of these introduced functions can be simplified significantly.

We plot functions $q(\alpha)$, $s(\alpha)$, $w_0(\alpha)$ and $w(\alpha)$ for several values of Pe, respectively in Figures 1–2.

It is clear from Figures 1-2 that function $q(\alpha)$, together with functions $s(\alpha)$ and $w_0(\alpha)$ are not sensitive to the value of Pe. In contrast, the function $w(\alpha)$ is highly dependent on Pe since the second term in the definition of $w(\alpha)$ has a coefficient $\frac{Pe}{4}$. Figure 2 shows that for small values of Pe, the function $w(\alpha)$ initially increases to a local maximum; after the local maximum $w(\alpha)$ decreases to a local minimum; after the local mininum $w(\alpha)$ starts to increase again. As the value of Pe increases, the locations of the maximum and minimum get closer. In other words, as the value of Pe increases, the zigzag part of $w(\alpha)$ shrinks. At a critical value of $Pe_c = 0.746027$, both the value and the location of the maximum coincide with those of the minimum, and the zigzag part of $w(\alpha)$ disappears. For $Pe > Pe_c$, function $w(\alpha)$ is monotonically increasing for $\alpha \in [-\frac{\pi}{4}, \frac{\pi}{4}]$.

Note that if we replace q in equation (17) by $q(\alpha)$ (and replace r by $r(\alpha)$), then equation (17) is an equation of α only where Pe and U are treated as parameters.

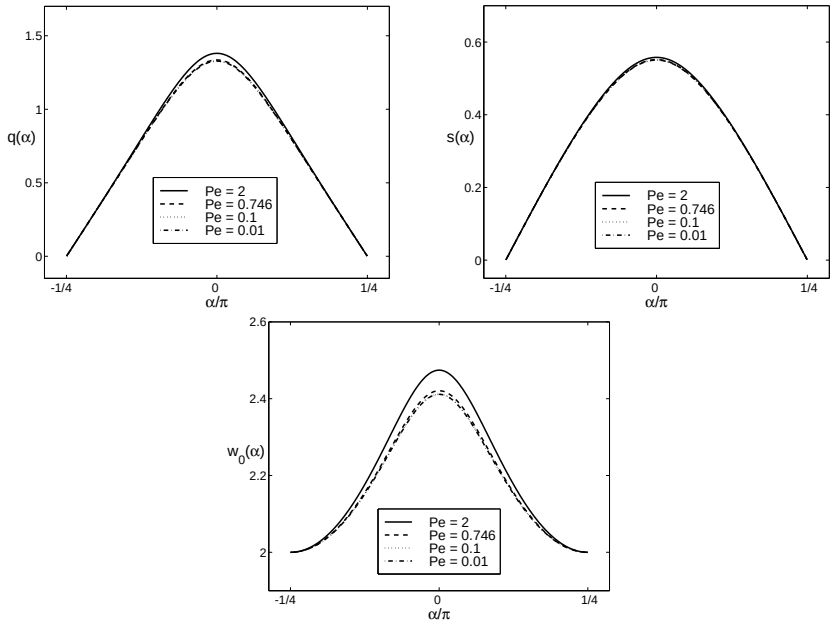

FIGURE 1. Functions $q(\alpha)$, $s(\alpha)$ and $w_0(\alpha)$ for various values of Pe.

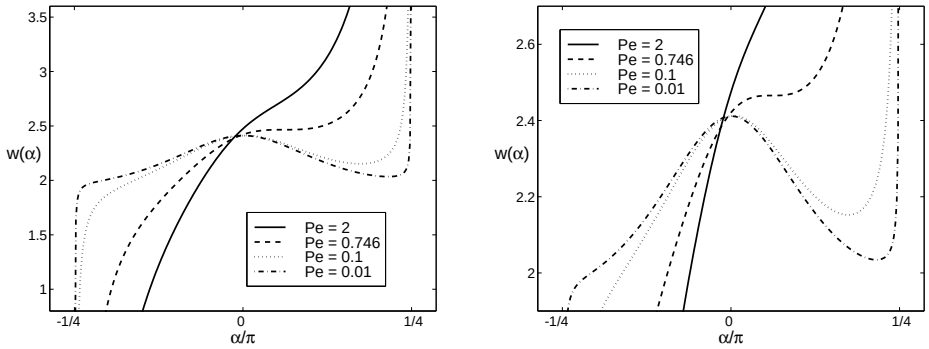

FIGURE 2. Function $w(\alpha)$ for various values of Pe. The right panel is a detailed view of the left panel.

In terms of function $w(\alpha)$, equation (17) becomes

$$w(\alpha, Pe) = U. \tag{20}$$

Here we write it as $w(\alpha, Pe)$ to show explicitly its dependence on Pe.

The phase diagram (steady states as functions of U or Pe or both) can be obtained by solving equation (20). As we discussed above, for $Pe < Pe_c$, equation (20) has one solution for small values of U; it has three solutions for U in an intermediate range; and it has one solution for large U. For $Pe > Pe_c$, the zigzag part of function $w(\alpha)$ disappears. As a result, for $Pe > Pe_c$, equation (20) has one

solution for any value of $U > 0$. Figure 3 shows the phase diagram (steady state as a function of U) for $Pe = 0.01$, corresponding to the case of weak shear. As shown in the figure, a cusp (actually it is smooth, see the insert in Figure 3) separates the diagram into two branches. As we argued in [31], the branch shown in solid line, which corresponds to the stable branch in the case of no shear ($Pe = 0$), is stable. The branch shown in dashed line is unstable [31]. The lower part of the dashed line branch corresponds to the unstable isotropic branch for $U > 2$ in the case of no shear ($Pe = 0$). The stability of the upper part of the dashed line branch was analyzed in our multi-scale asymptotic study [31]. In the case of weak shear (i.e. $Pe << 1$), a nematic equilibrium will keep its shape. But under the influence of weak shear ($Pe << 1$), its phase angle α will change with respect to the slow time scale $T_1 = Pe \cdot t$. The evolution of the phase angle α is governed by the differential equation [31]

$$\frac{d\alpha}{dT_1} = c_1(\sin^2\alpha + c_2), \tag{21}$$

where $c_1 > 0$. For $-1 < c_2 < 0$, the phase angle will converge to a steady state. The stability of a steady state phase angle α_0 is determined by the derivative of $\sin^2\alpha + c_2$ at α_0:

$$\frac{d}{d\alpha}(\sin^2\alpha + c_2) = 2\sin\alpha\cos\alpha = \sin 2\alpha.$$

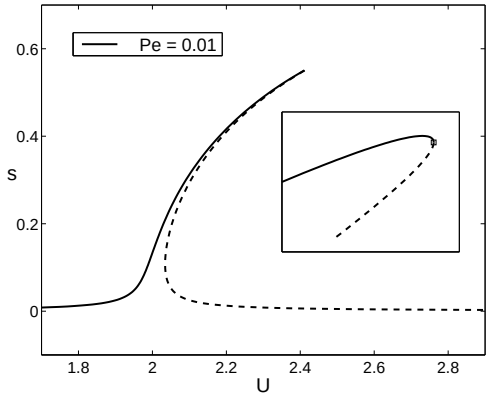

FIGURE 3. Phase diagram for $Pe = 0.01$. The insert is a magnified view of the cusp, which separates the phase diagram into two branches.

If $\sin 2\alpha_0 > 0$, then α_0 is unstable. If $\sin 2\alpha_0 < 0$, then α_0 is stable. As shown in Figure 4, for any $-1 < c_2 < 0$, there are two steady state phase angles in $(0, \pi)$. The one in $(\pi/2, \pi)$ is stable while the one in $(0, \pi/2)$ is unstable. The upper part of the dashed line branch in Figure 3 corresponds to the unstable steady state phase angle, and thus is unstable. In the asymptotic study of weak shear ($Pe << 1$) both the stable branch and the upper part of the unstable branch cease to exist for $U > U_c = 2.41144646$. For $U > U_c$, there is no steady state solution. Instead, there is a tumbling solution. In the analytical/numerical study here, the stable branch and the upper part of the unstable branch are connected to each other at the cusp (see the insert in Figure 3).

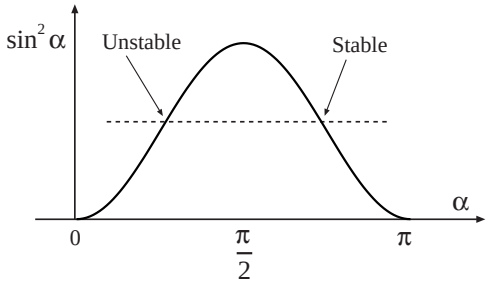

FIGURE 4. Stable and unstable steady state phase angles.

In Figure 5 we plot the phase diagram (steady state as a function of U) for several values of Pe.

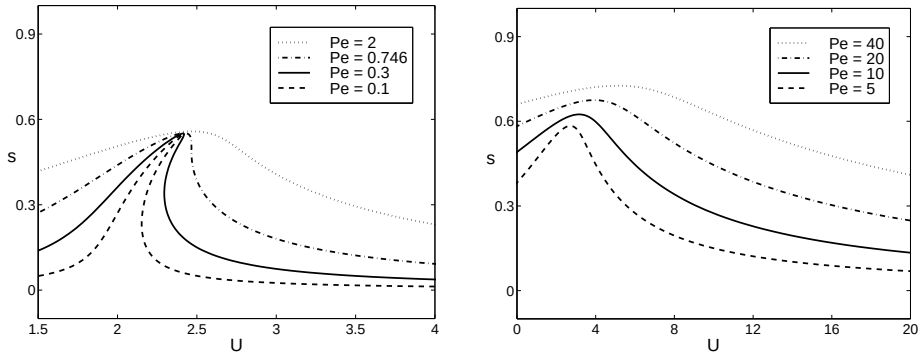

FIGURE 5. Left panel: Phase diagram for small-to-intermediate values of Pe. Right panel: Phase diagram for large values of Pe.

As shown in Figure 5, the cusp, which separates the phase diagram into two branches, is less and less well defined as the value of Pe increases. For $Pe > Pe_c$, the cusp disappears completely. Here it is important to point out that the system is not driven by a potential field because the effect caused by the shear flow is not a potential field. As a consequnce, a steady state branch may change its stability at any point even when it remains isolated. In contract, when a system is driven by a potential field, a steady state branch may change its stability only if some other branch bifurcates from it (or a fold occurs) [8].

4. **Stability study.** For a given value of Pe, a steady state solution is completely specified by the value of α. Once the value of α is known, U and the order parameter s are given by

$$U = w(\alpha),\ s = s(\alpha).$$

The probability density function (pdf) is calculated as follows:

$$\rho(\theta) \propto \exp[-\psi(\theta)] \int_0^\pi \exp\left[-\frac{Pe}{2}\bar{\theta} + \psi(\theta+\bar{\theta})\right] d\bar{\theta},$$

where the potential $\psi(\theta)$ is

$$\psi(\theta) = \frac{Pe}{4}\cos 2\alpha \sin 2\theta - q(\alpha)\cos 2\theta.$$

Since the pdf satisfies $\int_0^\pi \rho(\theta)d\theta = 1$ and is periodic with period π, it has the Fourier series expansion of the form

$$\rho(\theta) = \frac{2}{\pi}\left[\frac{1}{2} + \sum_{k=1}^{M}(a_k^{(0)}\cos 2k\theta + b_k^{(0)}\sin 2k\theta)\right], \tag{22}$$

where $b_1^{(0)} = 0$. We consider perturbations of the form

$$\Delta\rho(\theta,t) = \frac{2}{\pi}\sum_{k=1}^{M}\left[a_k(t)\cos 2k\theta + b_k(t)\sin 2k\theta\right]. \tag{23}$$

The Maier-Saupe interaction potential induced by the perturbed pdf $\bar{\rho}(\theta,t) \equiv \rho(\theta) + \varepsilon\Delta\rho(\theta,t)$ is

$$\bar{V}_{MS}(\theta) = -U\left[\langle\cos 2\theta\rangle\cos 2\theta + \langle\sin 2\theta\rangle\sin 2\theta\right],$$

where

$$\begin{aligned}
\langle\cos 2\theta\rangle &= \int_0^\pi \cos 2\theta\left[\rho(\theta) + \varepsilon\Delta\rho(\theta,t)\right]d\theta \\
&= a_1^{(0)} + \varepsilon\, a_1(t), \\
\langle\sin 2\theta\rangle &= \int_0^\pi \sin 2\theta\left[\rho(\theta) + \varepsilon\Delta\rho(\theta,t)\right]d\theta \\
&= \varepsilon\, b_1(t).
\end{aligned}$$

Substituting into the Maier-Saupe potential yields

$$\begin{aligned}
\bar{V}_{MS}(\theta) &= -Ua_1^{(0)}\cos 2\theta - \varepsilon U[a_1(t)\cos 2\theta + b_1(t)\sin 2\theta] \\
&= V_{MS}(\theta) + \varepsilon\Delta V_{MS}(\theta),
\end{aligned}$$

where $V_{MS}(\theta) = -Ua_1^{(0)}\cos 2\theta$ is the unperturbed Maier-Saupe interaction potential and $\Delta V_{MS}(\theta) = -U[a_1(t)\cos 2\theta + b_1(t)\sin 2\theta]$ is the perturbation to the Maier-Saupe potential. The perturbed pdf satisfies

$$\begin{aligned}
\frac{\partial(\rho+\varepsilon\Delta\rho)}{\partial t} &= \frac{\partial}{\partial\theta}\left[\left(-\frac{Pe}{2} + \frac{Pe}{4}V_{SH}^{'}(\theta) + V_{MS}^{'}(\theta)\right.\right. \\
&\quad \left.\left. + \varepsilon\Delta V_{MS}^{'}(\theta)\right)(\rho+\varepsilon\Delta\rho) + \frac{\partial}{\partial\theta}(\rho+\varepsilon\Delta\rho)\right].
\end{aligned}$$

Thus, $\Delta\rho(\theta,t)$ satisfies the linearized equation

$$\frac{\partial\Delta\rho}{\partial t} = \frac{\partial}{\partial\theta}\left[\left(-\frac{Pe}{2} + \frac{Pe}{4}V_{SH}^{'}(\theta) + V_{MS}^{'}(\theta)\right)\Delta\rho + \Delta V_{MS}^{'}(\theta)\rho(\theta) + \frac{\partial\Delta\rho}{\partial\theta}\right], \tag{24}$$

where

$$\begin{aligned}
-\frac{Pe}{2} + \frac{Pe}{4}V_{SH}^{'}(\theta) + V_{MS}^{'}(\theta) &= -\frac{Pe}{2} + \frac{Pe}{2}\cos 2\alpha\cos 2\theta + 2q(\alpha)\sin 2\theta, &(25)\\
\Delta V_{MS}^{'}(\theta) &= 2U[a_1(t)\sin 2\theta - b_1(t)\cos 2\theta]. &(26)
\end{aligned}$$

To further evaluate the terms in (24), we appeal to (23) and arrive at

$$\begin{aligned}
\cos 2\theta \cdot \Delta\rho &= \cos 2\theta \cdot \frac{2}{\pi} \sum_{k=1}^{M} [a_k(t) \cos 2k\theta + b_k(t) \sin 2k\theta] \\
&= \frac{2}{\pi} \sum_{k=1}^{M} \Bigg(a_k(t) \frac{1}{2} [\cos 2(k+1)\theta + \cos 2(k-1)\theta] \\
&\quad + b_k(t) \frac{1}{2} [\sin 2(k+1)\theta + \sin 2(k-1)\theta] \Bigg) \\
&= \frac{1}{\pi} [a_1(t) + a_2(t) \cos 2\theta + b_2(t) \sin 2\theta] \\
&\quad + \frac{1}{\pi} \sum_{k=2}^{M} ([a_{k-1}(t) + a_{k+1}(t)] \cos 2k\theta + [b_{k-1}(t) + b_{k+1}(t)] \sin 2k\theta) .
\end{aligned}$$

Similarly, we have

$$\begin{aligned}
\sin 2\theta \cdot \Delta\rho &= \frac{1}{\pi} [b_1(t) + b_2(t) \cos 2\theta - a_2(t) \sin 2\theta] \\
&\quad + \frac{1}{\pi} \sum_{k=2}^{M} ([b_{k+1}(t) - b_{k-1}(t)] \cos 2k\theta + [a_{k-1}(t) - a_{k+1}(t)] \sin 2k\theta) .
\end{aligned}$$

Using the expansion (22) and noting that $b_1^{(0)} = 0$, we find after some straightforward manipulations that

$$\begin{aligned}
\sin 2\theta \cdot \rho &= \sin 2\theta \cdot \frac{2}{\pi} \left[\frac{1}{2} + \sum_{k=1}^{M} (a_k^{(0)} \cos 2k\theta + b_k^{(0)} \sin 2k\theta) \right] \\
&= \frac{1}{\pi} \left[b_2^{(0)} \cos 2\theta + (1 - a_2^{(0)}) \sin 2\theta \right] \\
&\quad + \frac{1}{\pi} \sum_{k=2}^{M} \left[(b_{k+1}^{(0)} - b_{k-1}^{(0)}) \cos 2k\theta + (a_{k-1}^{(0)} - a_{k+1}^{(0)}) \sin 2k\theta \right] ,
\end{aligned}$$

and

$$\begin{aligned}
\cos 2\theta \cdot \rho &= \frac{1}{\pi} \left[a_1^{(0)} + (1 + a_2^{(0)}) \cos 2\theta + b_2^{(0)} \sin 2\theta \right] \\
&\quad + \frac{1}{\pi} \sum_{k=2}^{M} \left[(a_{k-1}^{(0)} + a_{k+1}^{(0)}) \cos 2k\theta + (b_{k-1}^{(0)} + b_{k+1}^{(0)}) \sin 2k\theta \right] .
\end{aligned}$$

From (22), (23), (25) and (26), we express quantity $I \equiv \left[-\frac{Pe}{2} + \frac{Pe}{4}V_{SH}^{'}(\theta) + V_{MS}^{'}(\theta)\right]\Delta\rho$ as

$$\begin{aligned}
I &= \left[-\frac{Pe}{2} + \frac{Pe}{2}\cos 2\alpha \cos 2\theta + 2q(\alpha)\sin 2\theta\right]\Delta\rho \\
&= \frac{1}{\pi}\left[-\frac{Pe}{2} + \frac{Pe}{2}\cos 2\alpha \cdot a_1(t) + 2q(\alpha)\cdot b_1(t)\right] \\
&\quad + \frac{1}{\pi}\left[-Pe\cdot a_1(t) + \frac{Pe}{2}\cos 2\alpha \cdot a_2(t) + 2q(\alpha)\cdot b_2(t)\right]\cos 2\theta \\
&\quad + \frac{1}{\pi}\left[-Pe\cdot b_1(t) + \frac{Pe}{2}\cos 2\alpha \cdot b_2(t) - 2q(\alpha)\cdot a_2(t)\right]\sin 2\theta \\
&\quad + \frac{1}{\pi}\sum_{k=2}^{M}\Bigg(-Pe\cdot a_k(t) + \frac{Pe}{2}\cos 2\alpha\cdot[a_{k-1}(t) + a_{k+1}(t)] \\
&\quad + 2q(\alpha)\cdot[b_{k+1}(t) - b_{k-1}(t)]\Bigg)\cos 2k\theta \\
&\quad + \frac{1}{\pi}\sum_{k=2}^{M}\Bigg(-Pe\cdot b_k(t) + \frac{Pe}{2}\cos 2\alpha\cdot[b_{k-1}(t) + b_{k+1}(t)] \\
&\quad + 2q(\alpha)\cdot[a_{k-1}(t) - a_{k+1}(t)]\Bigg)\sin 2k\theta,
\end{aligned}$$

and

$$\begin{aligned}
\Delta V_{MS}^{'}(\theta)\rho(\theta) &= 2U[a_1(t)\sin 2\theta - b_1(t)\cos 2\theta]\rho(\theta) \\
&= \frac{2U}{\pi}\left[-b_1(t)\cdot a_1^{(0)}\right] \\
&\quad + \frac{2U}{\pi}\left[a_1(t)\cdot b_2^{(0)} - b_1(t)\cdot(1 + a_2^{(0)})\right]\cos 2\theta \\
&\quad + \frac{2U}{\pi}\left[a_1(t)\cdot(1 - a_2^{(0)}) - b_1(t)\cdot b_2^{(0)}\right]\sin 2\theta \\
&\quad + \frac{2U}{\pi}\sum_{k=2}^{M}\left[a_1(t)\cdot(b_{k+1}^{(0)} - b_{k-1}^{(0)}) - b_1(t)\cdot(a_{k-1}^{(0)} + a_{k+1}^{(0)})\right]\cos 2k\theta \\
&\quad + \frac{2U}{\pi}\sum_{k=2}^{M}\left[a_1(t)\cdot(a_{k-1}^{(0)} - a_{k+1}^{(0)}) - b_1(t)\cdot(b_{k-1}^{(0)} + b_{k+1}^{(0)})\right]\sin 2k\theta.
\end{aligned}$$

Let

$$q_1 = \frac{Pe}{2}\cos 2\theta,\ q_2 = 2q(\alpha),\ q_3 = 2U.$$

Putting all these in the right hand side of (24) and simplifying, we get

$$\begin{aligned}
\text{RHS} &= \frac{2}{\pi}\Big[Pe\cdot b_1(t)+q_1b_2(t)-q_2a_2(t)-q_3[a_2^{(0)}-a_0^{(0)}]a_1(t)\\
&\quad -q_3[b_0^{(0)}+b_2^{(0)}]b_1(t)-4a_1(t)\Big]\cos 2\theta\\
&\quad +\frac{2}{\pi}\Big[Pe\cdot a_1(t)-q_1a_2(t)-q_2b_2(t)-q_3[b_2^{(0)}-b_0^{(0)}]a_1(t)\\
&\quad +q_3[a_0^{(0)}+a_2^{(0)}]b_1(t)-4b_1(t)\Big]\sin 2\theta\\
&\quad +\frac{2}{\pi}\sum_{k=2}^{M}k\,[-Pe\cdot b_k(t)+q_1[b_{k-1}(t)+b_{k+1}(t)]-q_2[a_{k+1}(t)-a_{k-1}(t)]\\
&\quad -q_3[a_{k+1}^{(0)}-a_{k-1}^{(0)}]\cdot a_1(t)-q_3[b_{k-1}^{(0)}+b_{k+1}^{(0)}]\cdot b_1(t)-4ka_k(t)\Big]\cos 2k\theta\\
&\quad +\frac{2}{\pi}\sum_{k=2}^{M}k\,[Pe\cdot a_k(t)-q_1[a_{k-1}(t)+a_{k+1}(t)]-q_2[b_{k+1}(t)-b_{k-1}(t)]\\
&\quad -q_3[b_{k+1}^{(0)}-b_{k-1}^{(0)}]\cdot a_1(t)+q_3[a_{k-1}^{(0)}+a_{k+1}^{(0)}]\cdot b_1(t)\\
&\quad -4kb_k(t)]\sin 2k\theta. \qquad (27)
\end{aligned}$$

Hence, from (24), it follows that the Fourier coefficients of the perturbation satisfy

$$\begin{aligned}
\frac{da_1(t)}{dt} &= -Pe\cdot b_1(t)+q_1b_2(t)-q_2a_2(t)-q_3[a_2^{(0)}-a_0^{(0)}]a_1(t)\\
&\quad -q_3[b_0^{(0)}+b_2^{(0)}]b_1(t)-4a_1(t),\\
\frac{db_1(t)}{dt} &= Pe\cdot a_1(t)-q_1a_2(t)-q_2b_2(t)-q_3[b_2^{(0)}-b_0^{(0)}]a_1(t)\\
&\quad +q_3[a_0^{(0)}+a_2^{(0)}]b_1(t)-4b_1(t),\\
\frac{da_k(t)}{dt} &= k\,[-Pe\cdot b_k(t)+q_1[b_{k-1}(t)+b_{k+1}(t)]-q_2[a_{k+1}(t)-a_{k-1}(t)]\\
&\quad -q_3[a_{k+1}^{(0)}-a_{k-1}^{(0)}]a_1(t)-q_3[b_{k-1}^{(0)}+b_{k+1}^{(0)}]b_1(t)-4ka_k(t)\Big],\\
\frac{db_k(t)}{dt} &= k\,[Pe\cdot a_k(t)-q_1[a_{k-1}(t)+a_{k+1}(t)]-q_2[b_{k+1}(t)-b_{k-1}(t)]\\
&\quad -q_3[b_{k+1}^{(0)}-b_{k-1}^{(0)}]a_1(t)+q_3[a_{k-1}^{(0)}+a_{k+1}^{(0)}]b_1(t)-4kb_k(t)\Big],
\end{aligned}$$

where we have set

$$a_0^{(0)}=1,\ b_0^{(0)}=0.$$

If we collect all of the Fourier coefficients of $\Delta\rho(\theta,t)$ into a vector

$$\mathbf{u}(t)=[a_1(t),b_1(t),a_2(t),b_2(t),\cdots,a_M(t),b_M(t)]^T,$$

then the above equations can be cast in a compact form

$$\frac{d\mathbf{u}(t)}{dt} = A[\rho(\theta)] \cdot \mathbf{u}(t), \tag{28}$$

where we have used the notation $A[\rho(\theta)]$ to show explicitly that the matrix A depends on the unperturbed steady state $\rho(\theta)$. If all of the eigenvalues of A have negative real parts, then the perturbation decays to zero as time goes to infinity and the steady state $\rho(\theta)$ is linearly stable; if at least one of the eigenvalues of A has a positive real part, then the steady state $\rho(\theta)$ is unstable. We use the Matlab package to solve this eigenvalue problem to determine the stability.

5. **Numerical results.** Referring to Figure 3, we showed the phase diagram with stability/instability indicated for the case of $Pe = 0.01$. In the figure, the solid line represents the stable branch and the dashed line represents the unstable branch. The numerical stability result is consistent with that of the asymptotic analysis. Numerical stability analysis shows that the stable and the unstable branches are connected at the folding point of the phase curve where the phase curve is vertical (i.e., the point where $\partial s/\partial U = \infty$). The transition point from the stable branch to the unstable branch can only be calculated from the numerical stability analysis. The asymptotic analysis is not capable of resolving this detail. Figure 6 shows the phase diagram with stability/instability indicated for the case of $Pe = 0.1$. The solid line represents the stable branch and the dashed line represents the unstable branch. Numerical stability analysis shows that the transition point from the stable branch to the unstable branch is the folding point of the phase curve where the phase curve is vertical (i.e. the point where $\partial s/\partial U = \infty$).

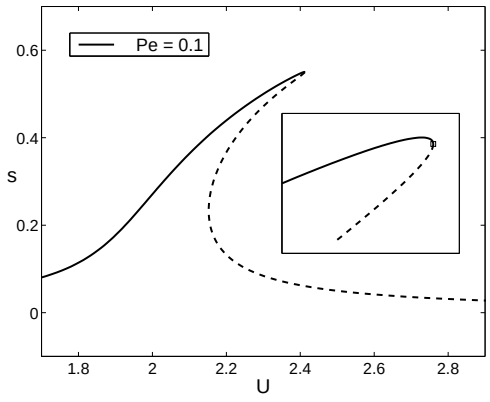

FIGURE 6. Phase diagram for $Pe = 0.1$.

In Figure 7 we show the phase diagrams with stability/instability indicated for several intermediate values of Pe. The solid line represents the stable branch and the dashed line represents the unstable branch. Numerical stability analysis shows that the transition from the stable branch to the unstable branch is the folding point of the phase curve if such a folding point exists. Note that this qualitative behavior based on the closure models has been observed in [21] even though they differ quantatively.

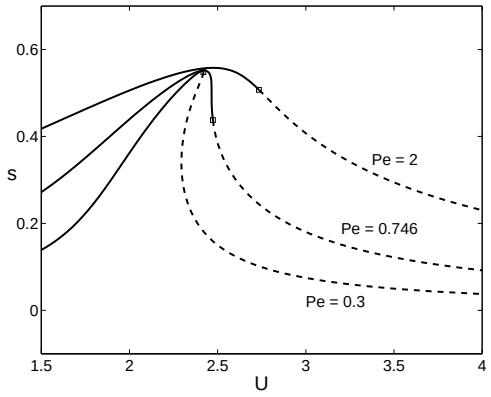

FIGURE 7. Phase diagram for intermediate values of Pe.

For $Pe < 0.746$, such a folding point exists. For $Pe > 0.746$, there is no such folding point. For $Pe > 0.746$, the transition from the stable branch to the unstable branch occurs at a point beyond the maximum.

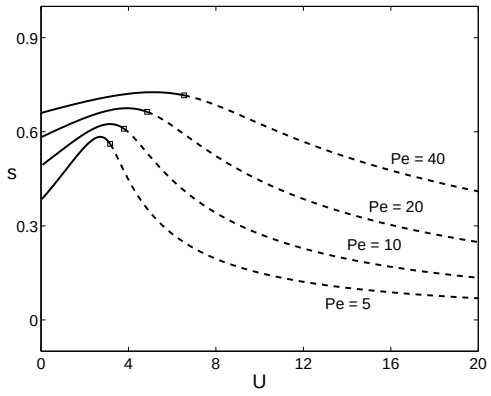

FIGURE 8. Phase diagram for large values of Pe.

Figure 8 depicts the phase diagram with stability/instability indicated for several large values of Pe. The solid line corresponds to the stable branch whereas the dashed line corresponds to the unstable branch. Numerical stability analysis indicates that the transition from the stable branch to the unstable branch occurs at a point beyond the maximum. Furthermore, as the value of Pe increases, the value (U) of the transition point increases.

Figure 9 describes the region of stable steady state (shaded) and the region of tumbling solution in the (U, Pe)-plane. This figure is also inherent in [21], where the locus of the Hopf bifurcation was shown. Here, it is captured from the kinetic theory.

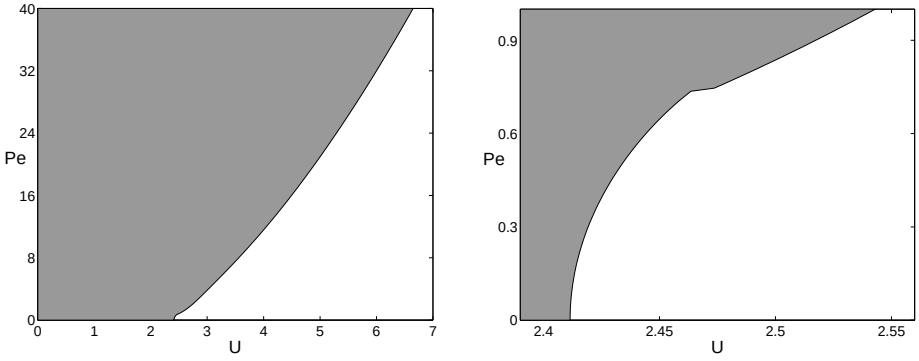

FIGURE 9. Region of stable steady state solution (shaded) and the region of tumbling solution. Left panel: overall view; Right panel: detailed view for small Pe.

6. **Conclusions.** We have semi-analytically investigated all steady state solutions and their stability for planar 2D nematic polymers under an imposed shear flow with arbitrary strength. We have confirmed the mesoscopic closure models of Lee *et al.* [21], extending their analysis and numerical studies to the Smoluchowski equation for the orientational probability distribution. A detailed phase diagram is given, consisting of all stable steady states versus the normalized concentration U and normalized shear rate or Peclet number Pe. Special attention has been given to the locus of bifurcations in the phase diagram where stable steady states no longer exist. These bifurcations are shown to consist of a fold among stable and unstable branches up to some critical Pe, after which the fold disappears and is replaced by Hopf bifurcation. Extension of the current work to 3-D model will be much more challenging mathematically.

Appendix A An efficient method for calculating $\int_0^\pi \exp\left[-f\bar{\theta}+\psi(\theta+\bar{\theta})\right] d\bar{\theta}$

Using the Fourier series expansion of $\exp(\psi(\theta)) = \sum_{k=-\infty}^{\infty} c_k \exp(ik2\theta)$, we obtain

$$\begin{aligned}
\int_0^\pi \exp\left[-f\bar{\theta}+\psi(\theta+\bar{\theta})\right] d\bar{\theta} &= \sum_{k=-\infty}^{\infty} c_k \int_0^\pi \exp\left[-f\bar{\theta}+ik2(\theta+\bar{\theta})\right] d\bar{\theta} \\
&= \sum_{k=-\infty}^{\infty} c_k \left[\int_0^\pi \exp\left[(-f+ik2)\bar{\theta}\right] d\bar{\theta}\right] \exp(ik2\theta) \\
&= \sum_{k=-\infty}^{\infty} c_k \frac{1-\exp(-f\pi)}{f-ik2} \exp(ik2\theta) \\
&= \sum_{k=-\infty}^{\infty} d_k \exp(ik2\theta),
\end{aligned}$$

where

$$d_k = c_k \frac{1-\exp(-f\pi)}{f-ik2}. \tag{29}$$

The numerical procedure for calculating $\int_0^\pi \exp\left[-f\bar{\theta}+\psi(\theta+\bar{\theta})\right] d\bar{\theta}$ is as follows.

- Apply FFT on $\psi(\theta)$ to calculate c_k.
- Calculate $d_k = c_k \dfrac{1-\exp(-f\pi)}{f-ik2}$.
- Apply IFFT on d_k to compute $\int_0^\pi \exp\left[-f\bar{\theta}+\psi(\theta+\bar{\theta})\right] d\bar{\theta}$.

Appendix B Existence of solution of $F_1(\alpha, q, Pe) \equiv \langle \sin 2\theta \rangle = 0$

We consider several cases.

Case 1: $q \to +\infty$

Since the pdf $\rho(\theta)$ given in (18) is periodic with period π, we can consider any interval of length π. Without loss of generality, let us select the interval $[-\frac{\pi}{2}, \frac{\pi}{2}]$. We have

$$\begin{aligned} F_1(\alpha, q, Pe) &\equiv \langle \sin 2\theta \rangle \\ &= \frac{1}{Z}\int_{-\frac{\pi}{2}}^{\frac{\pi}{2}}\int_0^\pi \sin 2\theta \exp\left[-\frac{\pi}{2}\bar{\theta}+\psi(\theta+\bar{\theta})-\psi(\theta)\right] d\bar{\theta}d\theta \\ &= \frac{1}{Z}\int_{-\frac{\pi}{2}}^{\frac{\pi}{2}}\int_0^\pi \sin 2\theta \exp\left[-\frac{Pe}{2}\bar{\theta}+\frac{Pe}{4}\cos 2\alpha[\sin 2(\theta+\bar{\theta})-\sin 2\theta]\right. \\ &\quad \left. -q[\cos 2(\theta+\bar{\theta})-\cos 2\theta]\right] d\bar{\theta}d\theta, \end{aligned} \tag{30}$$

where

$$\begin{aligned} Z &= \int_{-\frac{\pi}{2}}^{\frac{\pi}{2}}\int_0^\pi \exp\left[-\frac{Pe}{2}\bar{\theta}+\frac{Pe}{4}\cos 2\alpha[\sin 2(\theta+\bar{\theta})-\sin 2\theta]\right. \\ &\quad \left. -q[\cos 2(\theta+\bar{\theta})-\cos 2\theta]\right] d\bar{\theta}d\theta. \end{aligned}$$

For positive and large q, the dominant contribution in the above two integrals comes from a small region near $\theta = 0$ and $\bar{\theta} = \frac{\pi}{2}$. Away from this small region, the contribution is exponentially small.

In the inner integral with respect to $\bar{\theta}$, we make a change of variables $\bar{\theta}_{new} = \theta + \bar{\theta}$. For simplicity, we still use $\bar{\theta}$ to denote the new variable $\bar{\theta}_{new}$. Since the dominant contribution comes from a small region near $\theta = 0$ and $\bar{\theta} = \frac{\pi}{2}$, we can extend the integration limits away from the region of the dominant contribution. Specifically, we rewrite (30) as

$$
\begin{aligned}
& F_1(\alpha, q, Pe) \\
= \; & \frac{1}{Z}\int_{-\frac{\pi}{2}}^{\frac{\pi}{2}} \sin 2\theta \exp[\frac{Pe}{2}\theta - \frac{Pe}{4}\cos 2\alpha \sin 2\theta + q\cos 2\theta] \\
& \times \int_0^{\pi} \exp\left[-\frac{Pe}{2}(\theta+\bar{\theta}) + \frac{Pe}{4}\cos 2\alpha \sin 2(\theta+\bar{\theta}) - q\cos 2(\theta+\bar{\theta})\right] d\bar{\theta} d\theta \\
= \; & \frac{1}{Z}\int_{-\frac{\pi}{2}}^{\frac{\pi}{2}} \sin 2\theta \exp[\frac{Pe}{2}\theta - \frac{Pe}{4}\cos 2\alpha \sin 2\theta + q\cos 2\theta] \\
& \times \int_{\theta}^{\theta+\pi} \exp\left[-\frac{Pe}{2}\bar{\theta} + \frac{Pe}{4}\cos 2\alpha \sin 2\bar{\theta} - q\cos 2\bar{\theta}\right] d\bar{\theta} d\theta + T.S.T. \\
= \; & \frac{1}{Z}\int_{-\frac{\pi}{2}}^{\frac{\pi}{2}} \sin 2\theta \exp[\frac{Pe}{2}\theta - \frac{Pe}{4}\cos 2\alpha \sin 2\theta + q\cos 2\theta] \\
& \times \int_0^{\pi} \exp\left[-\frac{Pe}{2}\bar{\theta} + \frac{Pe}{4}\cos 2\alpha \sin 2\bar{\theta} - q\cos 2\bar{\theta}\right] d\bar{\theta} d\theta \\
& + T.S.T. \qquad (31)
\end{aligned}
$$

Here T.S.T. stands for transcendentally small term. Let

$$
C_1 = \int_0^{\pi} \exp\left[-\frac{Pe}{2}\bar{\theta} + \frac{Pe}{4}\cos 2\alpha \sin 2\bar{\theta} - q\cos 2\bar{\theta}\right] d\bar{\theta}. \qquad (32)
$$

We have

$$
\begin{aligned}
F_1(\alpha, q, Pe) &= \frac{C_1}{Z}\int_{-\frac{\pi}{2}}^{\frac{\pi}{2}} \sin 2\theta \exp[\frac{Pe}{2}\theta - \frac{Pe}{4}\cos 2\alpha \sin 2\theta + q\cos 2\theta] + T.S.T. \\
&= \frac{2C_1}{Z}\int_0^{\frac{\pi}{2}} \sin 2\theta \sinh\left(\frac{Pe}{2}\theta - \frac{Pe}{4}\cos 2\alpha \sin 2\theta\right) \exp(q\cos 2\theta) \\
&\quad + T.S.T. \qquad (33)
\end{aligned}
$$

We apply the Laplace method to the integral in (33). The dominant contribution comes from a small region near $\theta = 0$. To proceed, we need to find the leading term expansion of the part not containing q around $\theta = 0$. We discuss two cases.

Case 1A: $\cos 2\alpha < 1$

In this case, we have

$$
\sin 2\theta \sinh\left(\frac{Pe}{2}\theta - \frac{Pe}{4}\cos 2\alpha \sin 2\theta\right) = Pe(1-\cos 2\alpha)\theta^2 + \cdots,
$$

and

$$
\begin{aligned}
F_1(\alpha, q, Pe) &= \frac{2C_1}{Z}\int_0^{\frac{\pi}{2}} Pe(1-\cos 2\alpha)\theta^2 \exp\left[q(1-\frac{(2\theta)^2}{2})\right] d\theta + \cdots \\
&= \frac{2C_1}{Z}\exp(q) Pe(1-\cos 2\alpha)\int_0^{\infty} \theta^2 \exp[-2q\theta^2] d\theta + \cdots
\end{aligned}
$$

Introducing a change of variables

$$s = \theta^2, \;\; d\theta = \frac{1}{2\theta} ds = \frac{1}{2\sqrt{s}} ds,$$

we find

$$\begin{aligned} F_1(\alpha, q, Pe) &= \frac{C_1}{Z} \exp(q) Pe(1 - \cos 2\alpha) \int_0^\infty \sqrt{s} \exp[-2qs] ds + \cdots \\ &= \frac{C_1}{Z} \exp(q) Pe(1 - \cos 2\alpha) \frac{\frac{1}{2}\sqrt{\pi}}{2q\sqrt{2q}} + \cdots . \end{aligned} \tag{34}$$

Similarly, we get

$$\begin{aligned} Z &= 2C_1 \int_0^{\frac{\pi}{2}} \cosh(\frac{Pe}{2}\theta - \frac{Pe}{4} \cos 2\alpha \sin 2\theta) \exp(q \cos 2\theta) d\theta + T.S.T. \\ &= 2C_1 \exp(q) \int_0^\infty \exp(-2q\theta^2) d\theta + \cdots \\ &= C_1 \exp(q) \frac{\sqrt{\pi}}{\sqrt{2q}} + \cdots . \end{aligned} \tag{35}$$

Substituting (35) into (34) yields

$$F_1(\alpha, q, Pe) = Pe(1 - \cos 2\alpha) \frac{1}{4q} + \cdots > 0, \;\; \text{as } q \to +\infty.$$

Case 1B: $\cos 2\alpha = 1$

When $\cos 2\alpha = 1$, we have

$$\sin 2\theta \sinh(\frac{Pe}{2}\theta - \frac{Pe}{4} \cos 2\alpha \sin 2\theta) = \frac{2Pe}{3}\theta^4 + \cdots$$

and it follows that

$$\begin{aligned} F_1(\alpha, q, Pe) &= \frac{2C_1}{Z} \exp(q) \frac{2Pe}{3} \int_0^\infty \theta^4 \exp(-2q\theta^2) d\theta + \cdots \\ &= \frac{C_1}{Z} \exp(q) \frac{2Pe}{3} \int_0^\infty s\sqrt{s} \exp(-2qs) ds + \cdots \\ &= \frac{C_1}{Z} \exp(q) \frac{2Pe}{3} \frac{\frac{3}{4}\sqrt{\pi}}{(2q)^2\sqrt{2q}} + \cdots \end{aligned} \tag{36}$$

Combining (35) and (36), we obtain

$$F_1(\alpha, q, Pe) = \frac{Pe}{8q^2} + \cdots > 0, \;\; \text{as } q \to +\infty.$$

Case 2: $q \to -\infty$

This case is similar to Case 1 but simpler than it. The derivation is skipped. For negatively large q, the asymptotic result is

$$F_1(\alpha, q, Pe) = Pe(1 + \cos 2\alpha) \frac{1}{4q} + \cdots < 0, \;\; \text{as } q \to -\infty,$$

where we use the fact that the coefficient $(1 + \cos 2\alpha)$ is always positive for $\alpha \in [-\frac{\pi}{4}, \frac{\pi}{4}]$.

Acknowledgements. This work was partially supported by the Air Force Office of Scientific Research and by the National Science Foundation. The authors thank the anonymous referees for their constructive suggestions and comments on improving this manuscript.

REFERENCES

[1] B. Bird, R. C. Armstrong and O. Hassager, "Dynamics of Polymeric Liquids," vol. **1**, Wiley, 1987.

[2] C. V. Chaubal and L. G. Leal, *Smoothed particle hydrodynamics techniques for the solution of kinetic theory problems Part 2. The effect of flow perturbations on the simple shear behavior of LCPs*, J. Non-Newtonian Fluid Mech., **82** (1999), 25–55.

[3] P. Constantin, I. Kevrekidis and E. S. Titi, *Asymptotic states of a Smoluchowski equation*, Arch. Rat. Mech. Anal., **174** (2004), 365–384.

[4] P. Constantin, I. Kevrekidis and E. S. Titi, *Remarks on a Smoluchowski equation*, Discrete and Continuous Dynamical Systems, **11** (2004), 101–112.

[5] P. Constantin and J. Vukadinovic, *Note on the number of steady states for a 2D Smoluchowski equation*, Nonlinearity, **18** (2005), 441–443.

[6] A. M. Donald, A. H. Windle and S. Hanna, "Liquid Crystalline Polymers," 2^{nd} edition, Cambridge University Press, New York, 2006.

[7] M. Doi and S. F. Edwards, "The Theory of Polymer Dynamics," Oxford University Press, New York, 1986.

[8] I. Fatkullin and V. Slastikov, *Critical points of the Onsager functional on a sphere*, Nonlinearity, **18** (2005), 2565–2580.

[9] M. G. Forest, R. Zhou and Q. Wang, *Symmetries of the Doi kinetic theory for nematic polymers of arbitrary aspect ratio: at rest and in linear flows*, Phys. Rev. E, **66** (2002), 031712.

[10] M. G. Forest, Q. Wang and R. Zhou, *The flow-phase diagram of Doi-Hess theory for sheared nematic polymers II: finite shear rates*, Rheol. Acta, **44** (2004), 80–93.

[11] M. G. Forest, R. Zhou and Q. Wang, *The weak shear phase diagram for nematic polymers*, Rheol. Acta, **43** (2004), 17–37.

[12] M. G. Forest, R. Zhou and Q. Wang, *Chaotic boundaries of nematic polymers in mixed shear and extensional flows*, Physical Review Letters, **93** (2004), 088301–088305.

[13] M. G. Forest, R. Zhou and Q. Wang, *Kinetic structure simulations of nematic polymers in plane Couette cells, I: The algorithm and benchmarks*, SIAM MMS, **3** (2005), 853–870.

[14] M. G. Forest, R. Zhou and Q. Wang, *Scaling behavior of kinetic orientational distributions for dilute nematic polymers in weak shear*, J. Non-Newtonian Fluid Mech., **116** (2004), 183–204.

[15] M. G. Forest and Q. Wang, *Monodomain response of finite-aspect-ratio macromolecules in shear and related linear flows*, Rheol. Acta, **42** (2003), 20–46.

[16] stu M.G. Forest, S. Sircar, Q. Wang and R. Zhou, *Monodomain dynamics for rigid rod and platelet suspensions in strongly coupled coplanar linear flow and magnetic fields. II. Kinetic theory*, Physics of Fluids, **18** (2006), 103102.

[17] S. Z. Hess, *Fokker-Planck-equation approach to flow alignment in liquid crystals*, Z. Naturforsch. A, **31A** (1976), 1034–1037.

[18] S. Hess and M. Kroger, *Regular and chaotic orientational and rheological behaviour of liquid crystals*, J. Phys.: Condens. Matter, **16** (2004), S3835–S3859.

[19] G. Ji, Q. Wang, P. Zhang and H. Zhou, *Study of phase transition in homogeneous, rigid extended nematics and magnetic suspensions using an order-reduction method*, Physics of Fluids, **18** (2006), 123103.

[20] R. G. Larson, *Arrested tumbling in shearing flows of liquid crystal polymers*, Macromolecules, **23** (1990), 3983–3992.

[21] J. H. Lee, M. G. Forest and R. Zhou, *Alignment and rheo-oscillator criteria for sheared nematic polymer films in the monolayer limit*, Discrete and continuous dynamical systems-series B, **6** (2006), 339–356.

[22] H. Liu, H. Zhang and P. Zhang, *Axial symmetry and classification of stationary solutions of Doi-Onsager equation on the sphere with Maier-Saupe potential*, Comm. Math. Sci., **3** (2005), 201–218.

[23] C. Luo, H. Zhang and P. Zhang, *The structure of equilibrium solution of 1D Smoluchowski equation*, Nonlinearity, **18** (2005), 379–389.

[24] G. Marrucci and P. L. Maffettone, *Description of the liquid-crystalline phase of rodlike polymers at high shear rates*, Macromolecules, **22** (1989), 4076–4082.
[25] G. Marrucci and P. L. Maffettone, *Nematic phase of rodlike polymers. I. Prediction of transient behavior at high shear rates*, J. Rheol., **34** (1990), 1217–1230.
[26] A. D. Rey and M. M. Denn, *Dynamical phenomena in liquid-crystalline materials*, Annual Review of Fluid Mechanics, **34** (2002), 233–266.
[27] Q. Wang, S. Sircar and H. Zhou, *Steady state solutions of the Smoluchowski equation for rigid nematic polymers under imposed fields*, Comm. Math. Sci., **3** (2005), 605–620.
[28] A. Zarnescu, *The stationary 2D Smoluchowski equation in strong homogeneous flow*, Nonlinearity, **19** (2006), 1619–1628.
[29] H. Zhou, H. Wang, M. G. Forest and Q. Wang, *A new proof on axisymmetric equilibria of a three-dimensional Smoluchowski equation*, Nonlinearity, **18** (2005), 2815–2825.
[30] H. Zhou, H. Wang, Q. Wang and M. G. Forest, *Characterization of stable kinetic equilibria of rigid, dipolar rod ensembles for coupled dipole-dipole and Maier-Saupe potentials*, Nonlinearity, **20** (2007), 277–297.
[31] H. Zhou and H. Wang, *Steady states and dynamics of 2-D nematic polymers driven by an imposed weak shear*, Comm. Math. Sci., **5** (2007), 113–132.

Received December 2007; revised April 2008.

E-mail address: hongwang@ams.ucsc.edu
E-mail address: hzhou@nps.edu
E-mail address: forest@email.unc.edu